Article

Yuanhua Wu[1,†]
Jing Cai[1,†]
Bo Pang[1]
Liping Cao[1]
Qiankun He[2]
Qiansong He[1,*]
Anbang Zhang[1,*]

Bioinformatic Identification of Signaling Pathways and Hub Genes in Vascular Dementia

[1]Department of Neurology, The First Affiliated Hospital of Guizhou University of Traditional Chinese Medicine, 550002 Guiyang, Guizhou, China
[2]The First School of Clinical Medicine of Guizhou University of Traditional Chinese Medicine, 550001 Guiyang, Guizhou, China

Abstract

Background: Vascular dementia (VaD) is a prevalent neurodegenerative disease characterized by cognitive impairment due to cerebrovascular factors, affecting a significant portion of the aging population and highlighting the critical need to understand specific targets and mechanisms for effective prevention and treatment strategies. We aimed to identify pathways and crucial genes involved in the progression of VaD through bioinformatics analysis and subsequently validate these findings.

Methods: We conducted differential expression analysis, Weighted Gene Co-expression Network Analysis (WGCNA), Gene Ontology (GO), Kyoto Encyclopedia of Genes and Genomes (KEGG) pathway enrichment analysis, and Protein-Protein Interaction (PPI) analysis. We utilized pheochromocytoma 12 (PC12) cells to create an *in vitro* oxygen-glucose deprivation (OGD) model. We investigated the impact of overexpression and interference of adrenoceptor alpha 1D (*ADRA1D*) on OGD PC12 cells using TdT-mediated dUTP nick-end labeling (TUNEL), reverse transcription-quantitative polymerase chain reaction (RT-qPCR), western blot (WB), and Fluo-3-pentaacetoxymethyl ester (Fluo-3 AM) analysis.

Results: We found 187 differentially expressed genes (DEGs) in the red module that were strongly associated with VaD and were primarily enriched in vasoconstriction, G protein-coupled amine receptor activity, and neuroactive ligand-receptor interaction, mitogen-activated protein kinase (MAPK) signaling pathway, and cell adhesion. Among these pathways, we identified *ADRA1D* as a gene shared by vasoconstriction, G protein-coupled amine receptor activity, and neuroactive ligand-receptor interaction. The TUNEL assay revealed a significant decrease in PC12 cell apoptosis with *ADRA1D* overexpression ($p < 0.01$) and a significant increase in apoptosis upon silencing *ADRA1D* ($p < 0.01$). RT-qPCR and WB analysis revealed elevated ADRA1D expression ($p < 0.001$) and decreased phospholipase C beta (PLCβ) and inositol 1,4,5-trisphosphate receptor (IP3R) expression ($p < 0.05$) with *ADRA1D* overexpression. Moreover, the Fluo-3 AM assessment indicated significantly lower intracellular Ca^{2+} levels with *ADRA1D* overexpression ($p < 0.001$). Conversely, interference with *ADRA1D* yielded opposite results.

Conclusion: Our study provides a new perspective on the pathogenic mechanisms of VaD and potential avenues for therapeutic intervention. The results highlight the role of ADRA1D in modulating cellular responses to OGD and VaD, suggesting its potential as a target for VaD treatment.

Keywords

vascular dementia; oxygen-glucose deprivation; bioinformatics analysis; hub genes; ADRA1D

Introduction

Vascular dementia (VaD) is a clinical syndrome characterized by brain tissue damage and cognitive impairment that occurs after a series of cerebrovascular diseases such as stroke [1]. Approximately 50 million individuals worldwide are currently afflicted with dementia, and the number of VaD patients is projected to triple by 2050 [2]. The

*Corresponding author details: Qiansong He, Department of Neurology, The First Affiliated Hospital of Guizhou University of Traditional Chinese Medicine, 550002 Guiyang, Guizhou, China. Email: hqs0820@126.com; Anbang Zhang, Department of Neurology, The First Affiliated Hospital of Guizhou University of Traditional Chinese Medicine, 550002 Guiyang, Guizhou, China. Email: 544820318@qq.com
†These authors contributed equally.

prevalence of VaD is increasing in the elderly population, with at least 20% of dementia cases attributed to vascular dementia, ranking second only to Alzheimer's disease (AD) [3]. VaD leads to declines in cognitive function, memory, and executive abilities, which not only severely impacts the well-being of individuals but also jeopardizes their health, making it a significant global public health challenge [4]. Researches have indicated that cerebrovascular disease is the core cause of VaD, and risk factors such as smoking, drinking, hypertension, hyperlipidemia, hyperglycemia, hyperhomocysteinemia, heart disease, and diabetes are also closely associated with VaD occurrence [5,6]. The pathogenesis of VaD is complex and has not yet been fully elucidated. It may be related to oxidative stress, cell apoptosis, inflammatory responses, blood-brain barrier damage, chronic hypoperfusion, and hypoxia [7–9]. Currently, the treatment of VaD relies primarily on clinical data, cognitive function tests, and pathological examinations [10]. However, there is a lack of ideal drugs or therapies that can effectively improve or reverse VaD progression. Hence, it is imperative to explore the molecular functions of VaD and to identify promising indicators for treatment.

Bioinformatics analysis of transcriptome data to identify biomarkers and elucidate the mechanisms underlying various diseases, including dementia and VaD, has been extensively investigated [11,12]. Research has shown that inflammatory responses significantly impact the development of VaD, and specific biomarkers associated with inflammation have emerged as potential indicators [13]. Interleukin-1 beta (IL-1β) accelerates the release of other inflammatory cytokines, generates inflammatory metabolites, promotes leukocyte migration, and further damages neurons, leading to the development of VaD [14]. Interleukin-6 (IL-6) is also a potential inflammatory biomarker and may serve as a novel marker for distinguishing AD and VaD [15]. Additionally, oxidative stress is considered a pathogenic mechanism involved in VaD [16]. Malondialdehyde (MDA), a product of lipid reactions with oxygen-free radicals during the oxidation process, has been identified as a reliable biomarker of oxidative damage [17]. Studies have indicated that dynamic monitoring of serum MDA levels can provide essential data for assessing the severity and prognosis of patients [18]. However, there is currently a lack of reported biomarkers to diagnose VaD, highlighting the need for large-scale research and clinical validation to identify such biomarkers.

In this study, we examined the gene expression data of frontal cortex samples in the VaD microarray dataset to identify differentially expressed genes (DEGs) between VaD and normal samples. Weighted Gene Co-expression Network Analysis (WGCNA) was conducted to investigate and describe various gene combinations and correlations among samples and identify DEGs in the key module associated with VaD. Gene Ontology (GO) and Kyoto Encyclopedia of Genes and Genomes (KEGG) pathway enrichment analyses were carried out to determine the biological processes of DEGs in the key module. Additionally, Protein-Protein Interaction (PPI) analysis was conducted to reveal potential interactions among proteins encoded by DEGs and identify key genes. Finally, through interference and overexpression experiments, the effects of candidate genes in an oxygen-glucose deprivation (OGD) model cell model were assessed using TdT-mediated dUTP nick end labeling (TUNEL), reverse transcription-quantitative polymerase chain reaction (RT-qPCR), western blot (WB), and Fluo-3-pentaacetoxymethyl ester (Fluo-3 AM) methods. Our extensive bioinformatics and molecular biology analyses revealed the molecular characteristics of VaD, offering novel insights into the underlying mechanisms and potential therapeutic targets.

Materials and Methods

Data Collection

Gene expression information was downloaded from NCBI's Gene Expression Omnibus (GEO) database (https://www.ncbi.nlm.nih.gov/geo/). The GSE122063 dataset contains gene expression data of frontal cortex samples from 8 VaD patients and 11 controls.

Analysis of Differential Gene Expression

DEG analysis on the GSE122063 dataset was conducted to identify DEGs in VaD versus matched controls using the R package of DEseq2 software (version 1.31.2, European Molecular Biology Laboratory, Heidelberg, Germany). The fold change (FC) based on Fragments Per Kilobase of transcript per Million mapped reads (FPKM) values was calculated to determine differential expression levels. DEGs meeting the conditions of $|\log_2 FC| > 1$ and adjusted p-value of <0.05 were regarded as statistically significant. The expression of DEG was visualized using a volcano plot and heatmap, then was standardized using the "normalize between arrays" function of the R software (version 4.2.1, Lucent Technologies Inc., Union, NJ, USA, https://www.r-project.org/) and visualized with a box plot. Using R software, we conducted principal component analysis (PCA) on the dataset and visualized the results.

WGCNA

We used the "WGCNA" package in R software to build a co-expression network and identify gene modules highly correlated with VaD. In this study, 634 DEGs were used for WGCNA analysis. A soft threshold value of 4 was applied to construct an adjacency matrix from the DEGs, which was then transformed into a topological overlap matrix. Hierarchical clustering and dynamic tree cutting were used to identify gene modules, merging similar modules with a height merge threshold of 0.25. We calculated gene significance (GS) and module significance (MS) to assess the association and significance between genes in biological modules and clinical information.

GO Function and Pathway Enrichment Analyses

To further explore the gene functions associated with VaD, we performed Gene Ontology (GO) function (http://www.geneontology.org/) and KEGG pathway enrichment (http://www.genome.jp/kegg/) on the gene modules most correlated with VaD. We employed R 3.6.1 software along with "biological conductor" and "goplot" software packages, considering results significant at $p < 0.05$. GO functional enrichment analysis included three major categories: molecular functions (MF), biological processes (BP), and cellular components (CC).

PPI Network Analysis

To investigate the PPI relationships of genes within the WGCNA modules, we used the STRING database (http://www.string-db.org) to establish the PPI network. Information from the PPI network was loaded into the Cytoscape software to identify key gene nodes within the modules (version 3.6.1, The Cytoscape Consortium, New York, NY, USA).

Construction of Adrenoceptor Alpha 1D (ADRA1D) Plasmids

Plasmids for *ADRA1D* interference and overexpression were constructed by Chongqing Biomedicine Biotechnology Co., Ltd., (Chongqing, China). The *ADRA1D* interference target was ligated onto the linearized pLVX-shRNA2-Luc-puro vector, while the *ADRA1D* gene's target sequence was connected to the pLVX-IRES-puro vector. The interference target sequence and overexpression sequence for *ADRA1D* are provided in **Supplementary Tables 1,2**.

Cell Culture and Grouping

Rat adrenal pheochromocytoma cells (PC12, SNL-124) were obtained from Wuhan Shengen Biological (Wuhan, China). They were cultured in Roswell Park Memorial Institute (RPMI) 1640 medium (L110KJ, Basalmedia Biotechnology, Shanghai, China) supplemented with 10% Fetal Bovine Serum (FBS) (AC03L055, LiJi Biotech, Shanghai, China) and 1% penicillin-streptomycin (C0009, Beyotime, Shanghai, China) in a CO_2 incubator at 37 °C. The logarithmic growth phase cells were taken at generation P3 to construct an *in vitro* oxygen-glucose deprivation (OGD) model. When the cells reached 60%–70% confluence under normal culture conditions, the medium was replaced with Earle's balanced salt solution, and the cells were incubated in a hypoxic chamber (94% N_2, 5% CO_2, 1% O_2, 37 °C) for 2 hours. Subsequently, the medium was replaced with fresh Dulbecco's Modified Eagle Medium (DMEM) (C11995500BT, Thermo Fisher Scientific, Waltham, MA, USA) [19]. The cells were divided into different groups: *ADRA1D* overexpression empty vector group (OE-*ADRA1D* NC), *ADRA1D* overexpression group (OE-*ADRA1D*), *ADRA1D* interference empty vector group (sh-*ADRA1D* NC), and *ADRA1D* interference group (sh-*ADRA1D*). Plasmids corresponding to each group were transfected into PC12 cells using Lentifusion Nanofusion version 2.0 (1019-014, Biomedicine Biotechnology, Chongqing, China). To prepare the transfection mixture, plasmids for each group and Lentifusion Nanofusion version 2.0 were dissolved in 490 µL Optimized Minimal Essential Medium (OPTI-MEM) (31985070, Thermo Fisher Scientific, Waltham, MA, USA). After incubating at room temperature for 5 minutes, the mixture was added to the culture dish, thoroughly mixed, and then placed in the incubator for further cultivation. It was confirmed that all cell lines were no contamination with mycoplasma.

TUNEL Detection of Cell Apoptosis

Cell slides fixed with 4% paraformaldehyde (DF0135, Leagene Biotechnology Co., Ltd., Beijing, China) were washed with Phosphate-Buffered Saline (PBS) (G0002, Servicebio Biotechnology, Wuhan, China). A suitable amount of 0.3% Triton X-100 permeabilization solution (T795, Beyotime Biotechnology, Shanghai, China) was added to the slides. Subsequently, TUNEL staining was performed according to the instructions of the one-step TUNEL apoptosis detection kit (FITC green fluorescence) (G1501, Sevier Biotechnology Co., Ltd., Wuhan, China). Detection solution (TdT enzyme: fluorescent labeling solution = 1:9) was added by drops, and the samples were incubated at 37 °C for 1 hour in the dark. After one cycle of

PBS washing, 4′,6-diamidino-2-phenylindole (DAPI) was added in drops to stain for 5 minutes, and slides were dehydrated and mounted with neutral resin (10004160, Sinopharm, Beijing, China). Image acquisition of the slices was conducted using a Mshot inverted microscope (MF53, Guangzhou Mingmei Photoelectric Technology Co., Ltd., Guangzhou, China). The nuclei of apoptotic cells emitted green fluorescence, while the DAPI-stained nuclei emitted blue fluorescence.

RT-qPCR

Total RNA extraction was performed using TRIzol reagent (15596026, Thermo Fisher Scientific, Inc., Waltham, MA, USA) [20], following the manufacturer's instructions. Reverse transcription was carried out according to the Goldenstar™ RT6 cDNA Synthesis Kit Ver.2 (TSK302M, Tsingke Biotechnology Co., Ltd., Beijing, China) protocol. mRNA expression was assessed using the 2× T5 Fast RT-qPCR Mix (SYBR Green I) kit (TSE002, Tsingke Biotechnology Co., Ltd., Beijing, China) with the following reaction conditions: 95 °C for 30 seconds, 95 °C for 5 seconds, 60 °C for 30 seconds, for 40 cycles. Glyceraldehyde-3-phosphate dehydrogenase (*GAPDH*) served as the internal reference gene, and the relative gene expression was calculated using the $2^{-\Delta\Delta Ct}$ method. Specific primers for RT-qPCR are provided in **Supplementary Table 3**.

Western Blot

Total cellular protein was extracted using Radio-Immunoprecipitation Assay (RIPA) lysis buffer (P0013B, Beyotime, Shanghai, China) containing Phenylmethylsulfonyl fluoride (PMSF) and a cocktail of protease inhibitors. Protein samples from each group were mixed with 5× SDS Loading Buffer (8015011, DAKEWE Biotechnology, Shenzhen, China) in a 4:1 ratio and denatured by heating at 100 °C for 6 minutes in a metal bath. Subsequently, 20 µL of each protein sample underwent 10% Sodium Dodecyl Sulfate Polyacrylamide Gel Electrophoresis (SDS-PAGE) electrophoresis (PG112, Epizyme Biology, Shanghai, China) for 90 minutes, followed by protein transfer to a Polyvinylidene Difluoride (PVDF) membrane (10600023, Amersham, Germany). After transfer, the membrane was blocked with 5% skimmed milk at room temperature for 1 hour. Primary antibodies, namely phospholipase C beta (PLCβ) (A22526), inositol 1,4,5-trisphosphate receptor (IP3R) (A4436), and GAPDH (AS014) obtained from ABclonal Technology (Wuhan, China), and ADRA1D (ab166925) acquired from Abcam Technology (Shanghai, China), were diluted 1:1000 and incubated overnight at 4 °C. The membrane was then incubated with the secondary antibody, HRP Goat Anti-Rabbit IgG antibody (AS014, ABclonal Technology, Shanghai, China), diluted 1:2000, at room temperature for 1 hour. Enhanced Chemiluminescence (ECL) exposure solution (34580, Thermo Fisher Scientific, Inc., Waltham, MA, USA) was uniformly applied to the membrane, and detection was carried out using a nucleic acid and protein gel imaging system (Universal Hood II, Bio-Rad, Hercules, CA, USA). Grayscale values of the bands were determined using ImageJ (version 1.48b, National Institutes of Health, Bethesda, MD, USA).

Measurement of Intracellular Ca^{2+} Levels Using Fluo-3-pentaacetoxymethyl Ester (Fluo-3 AM)

PC12 cells were collected, and Fluo-3 AM (S1056, Beyotime Biotechnology, Shanghai, China) was added to achieve a final concentration of 5 µM. The cells were then incubated at 37 °C for 60 minutes. Afterward, the cells were washed three times with cell staining buffer, followed by the addition of 500 µL of staining buffer. The cells were further incubated at 37 °C for 30 minutes to ensure complete conversion of Fluo-3 AM to Fluo-3 within the cells. Subsequently, flow cytometry (Beamcyte-1026M, Beamdiag Biotechnology, Changzhou, China) was employed for detection.

Statistical Analysis

Descriptive statistical values for experimental data were presented as mean ± standard deviation. Statistical analyses, including one-way analysis of variance (ANOVA) and Tukey's post hoc test, were performed using GraphPad Prism (version 8.0, GraphPad Company, San Diego, CA, USA). A level of $p < 0.05$ was considered as statistically significant difference.

Results

Differential Gene Expression Analysis and Distinct Expression Patterns in VaD

In this study, the genetic expression dataset GSE122063 was chosen, and 634 DEGs were detected, comprising 276 upregulated genes and 358 downregulated genes (Fig. 1A). The heatmap revealed the levels of expression of the top 50 DEGs, which were accurately distinguished between the control and VaD samples based on distinct expression patterns, indicating the reliability of the results for subsequent analysis (Fig. 1B). Before

further analysis, the expression data of the DEGs from GSE122063 were normalized and visualized using a box plot (Fig. 1C). The signal box blot demonstrates a uniform signal intensity distribution in all the samples. Principal component analysis (PCA) was then used to condense the dimensionality of the data and display different genetic expression patterns between the control and VaD groups (Fig. 1D).

Identification of Hub Modules with WGCNA

Based on the systems biology approach of WGCNA, a gene co-expression network was constructed for the GSE122063 dataset to screen potential genes associated with VaD. The results of WGCNA indicate that when selecting the appropriate soft threshold power, the gene co-expression network exhibits scale-free characteristics, meaning that the network structure demonstrates similar topological features at different scales. The network topology analysis was performed with a threshold of 4 (Fig. 2A). Fig. 2B indicates that the mean connectivity varies significantly across soft threshold powers. This variation reflects gene co-expression network density changes and structural characteristics under different soft threshold settings. Each branch of the dendrogram corresponds to a different gene module, and each leaf on the dendrogram represents a gene in which similar genes are clustered into modules of the same color. The dynamic tree-cut method was employed to identify gene modules, and highly similar modules were merged, resulting in 32 modules (Fig. 2C). A correlation heatmap of the modules and clinical traits is plotted (Fig. 3A). Eight modules showed significant associations with VaD: black (0.002), blue (9×10^{-4}), red (2×10^{-6}), brown (0.02), cyan (7×10^{-4}), dark turquoise (0.007), sky blue (0.01), and dark green (0.04). Among these, the red module exhibited the strongest correlation with the clinical phenotype of VaD (r = 0.86). In addition, module membership versus gene significance results are shown in Fig. 3B, illustrating that the red module was closely related to the VaD (cor = 0.87, $p < 1 \times 10^{-200}$). The red module was designated as the key gene module, containing 767 genes, and a Venn diagram revealed 187 overlapping DEGs (Fig. 3C).

Functional and Pathway Enrichment Analysis of DEGs in the Hub Module

We performed GO and KEGG enrichment analyses to identify the functional and pathway enrichment of VaD-related DEGs. The results of GO and KEGG analyses were ranked in descending order of *p*-value, and the top 10 most significant results were selected and plotted using the R software. GO analysis results showed that BP was mainly focused on the regulation of organelle assembly, vasoconstriction mRNA cis splicing via spliceosome, and mitochondrial protein processing, such as Heat Shock Protein Family A Member 1A (*HSPA1A*), Small Mothers Against Decapentaplegic 4 (*SMAD4*), and *ADRA1D*; CC was mainly focused on neuron projection cytoplasm, Transport Protein Particle (TRAPP) complex, vesicle tethering complex, axon cytoplasm, spliceosomal complex, and Gamma-Aminobutyric Acid (GABA)-ergic synapse, such as Heat Shock Protein Family B (Small) Member 1 (*HSPB1*) and Trafficking Protein Particle Complex 2-Like (*TRAPPC2L*); MF was mainly focused on Adenosine Triphosphate (ATP) hydrolysis activity, peptidyl-proline dioxygenase activity, protein folding chaperone, and G protein-coupled amine receptor activity, such as *HSPA1A*, Prolyl 4-Hydroxylase Subunit Alpha 1 (*P4HA1*), *HSPB1* and *ADRA1D* (Fig. 4A). The KEGG pathways involved were mainly arginine and proline metabolism, neuroactive ligand-receptor interaction, DNA replication, adherens junction, neurotrophin signaling pathway, mitogen-activated protein kinase (MAPK) signaling pathway, such as *P4HA1*, Prolyl 4-Hydroxylase Subunit Alpha 2 (*P4HA2*), *ADRA1D*, Replication Factor C Subunit 3 (*RFC3*), and *SMAD4* (Fig. 4B).

PPI Network Construction and Identification of Hub Genes

The PPI between the hub genes were derived from the STRING database (https://string-db.org/) and are shown in Fig. 5. STRING is a database that collects information on known and predicted protein functional associations from multiple sources [21]. Among the 187 DEGs in the red module, 18 genes were found to have protein–protein interactions, including Fanconi Anemia Complementation Group C (*FANCC*), *HSPA1A*, *HSPB1*, Leucine Proline-Enriched Proteoglycan (Leprecan) Like 1 (*LEPREL1*), Mitogen-Activated Protein Kinase Kinase 3 (*MAP2K3*, *MAP3K3*), *P4HA1*, *P4HA2*, Prohibitin 2 (*PHB2*), Pre-MRNA Processing Factor 4B (*PRPF4B*), Replication Factor C Subunit 3 (*RFC3*), Squamous Cell Carcinoma Antigen Recognized by T Cells 1 (*SART1*), *SMAD4*, Spastic Paraplegia 7 (*SPG7*), Serine/Threonine Kinase 11 Interacting Protein (*STK11IP*), Trafficking Protein Particle Complex 12 (*TRAPPC12*), *TRAPPC2L*, and Trafficking Protein Particle Complex 9 (*TRAPPC9*), which were considered candidate hub genes.

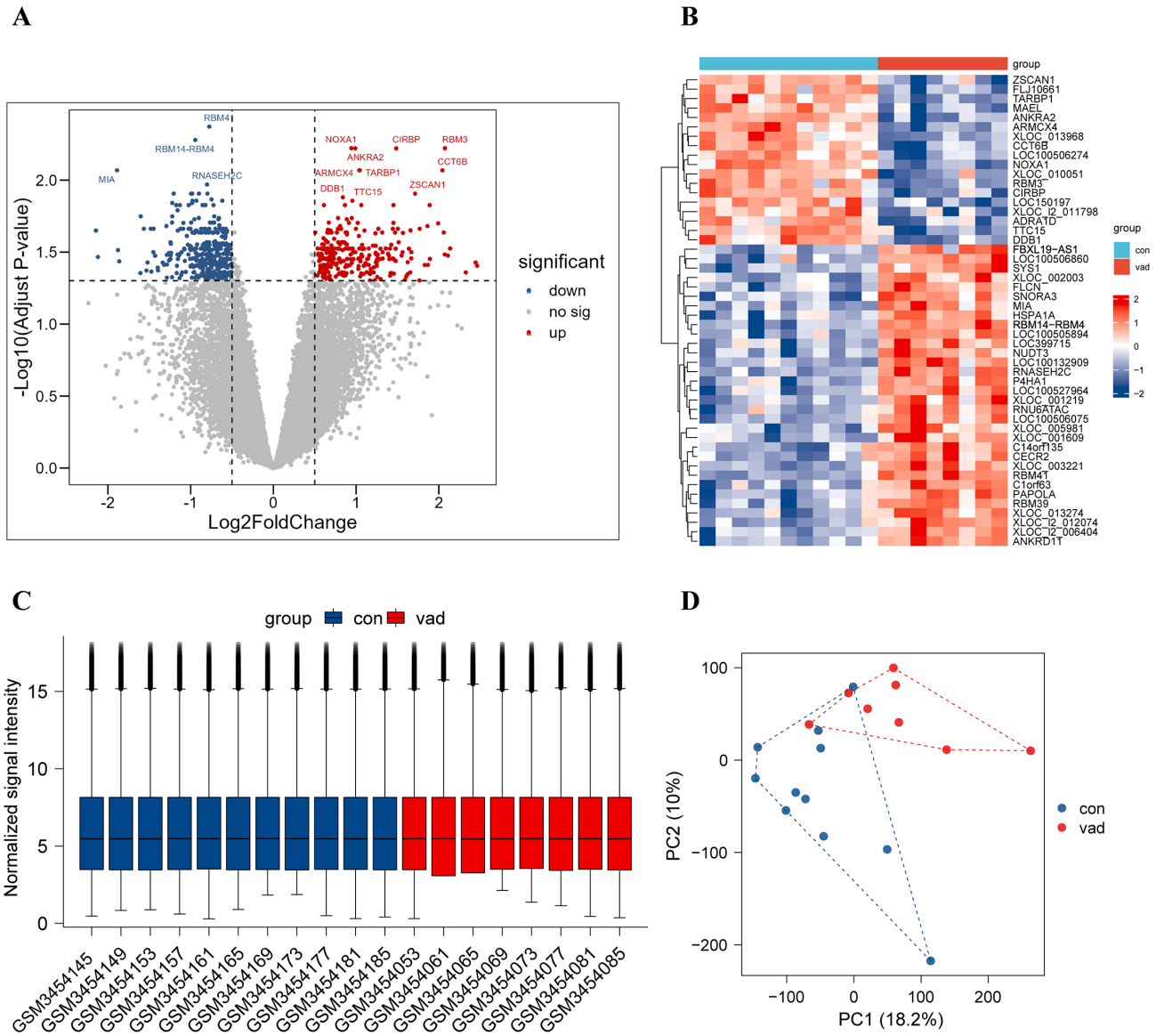

Fig. 1. Analysis of differentially expressed genes (DEGs) in the dataset GSE122063. (A) Volcano plot of DEGs. Colors toward blue indicate downregulated DEGs, colors toward red indicate upregulated DEGs, and gray represents non-significantly DEGs. (B) Hierarchical clustering heatmap of the top 50 DEGs. Colors toward blue indicate downregulated DEGs, colors toward red indicate upregulated DEGs. (C) Box plot of the DEGs expression data after normalization. (D) Principal component analysis (PCA) plot. The blue points represent the control samples, and the red points represent Vascular dementia (VaD) samples. VaD, vascular dementia samples; con, control samples.

Identification of ADRA1D as a Potential Therapeutic Target in Vascular Dementia

ADRA1D was selected as a candidate gene from signaling pathways associated with VaD, including vasoconstriction, G protein-coupled amine receptor activity, and the neuroactive ligand-receptor interaction. Simultaneously, *ADRA1D* showed significant differential expression in the dataset. The impact of *ADRA1D* was validated through both overexpression and interference experiments. In TUNEL experiments, the nuclei of apoptotic cells were stained in brownish-yellow, while the nuclei of normal negative cells were stained in blue. The results revealed a notable suppression of PC12 cell apoptosis with the overexpression of *ADRA1D* ($p < 0.01$), contrasting with a significant increase of apoptosis upon silencing *ADRA1D* ($p < 0.01$) (Fig. 6A). Additionally, RT-qPCR results demonstrated a substantial elevation in *ADRA1D* expression in PC12 cells following

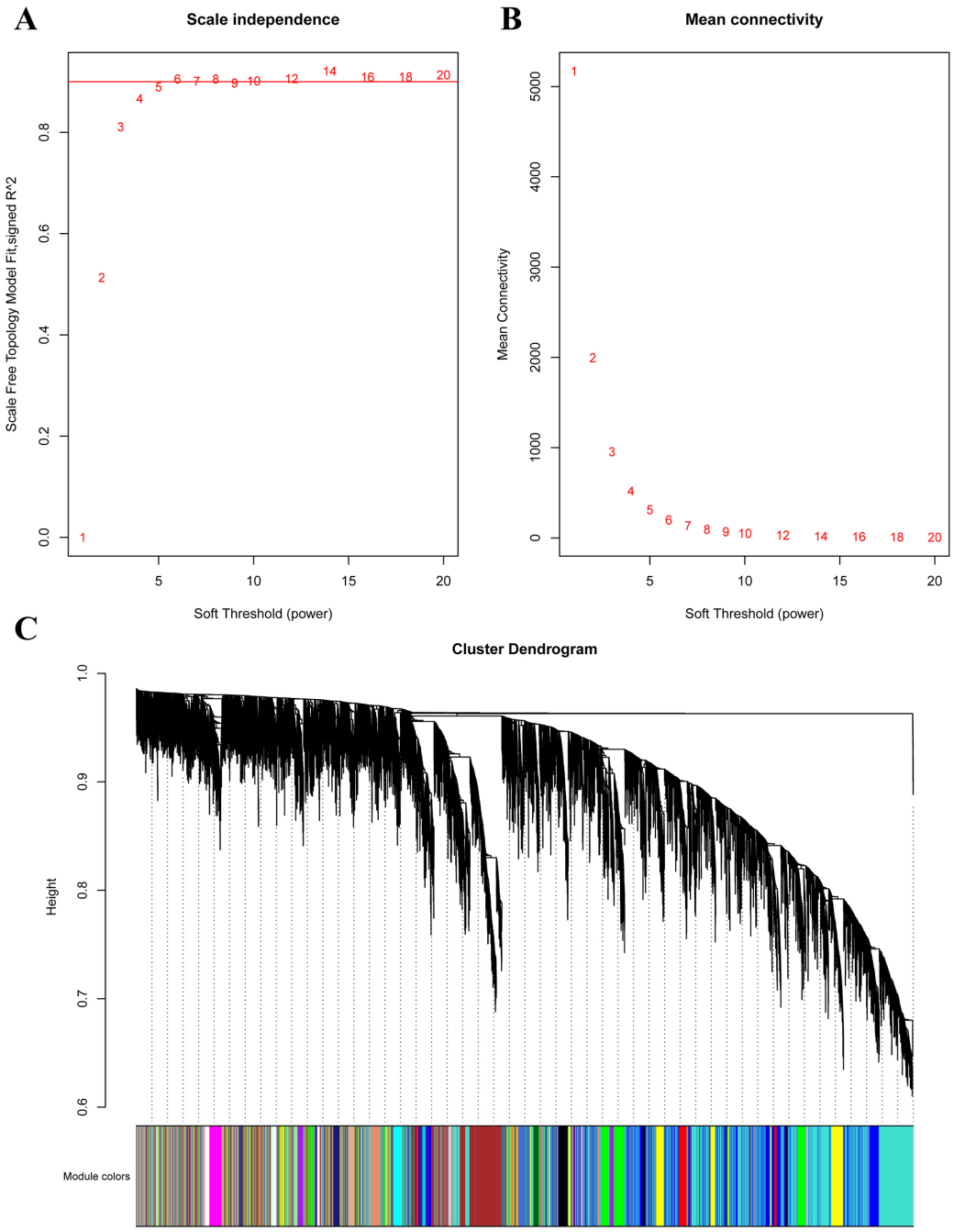

Fig. 2. Construction of gene co-expression networks using Weighted Gene Co-expression Network Analysis (WGCNA). (A) Analysis of scale independence. (B) Mean connectivity for different soft threshold powers. (C) Cluster dendrogram of all differentially expressed genes clustered based on a dissimilarity measure.

ADRA1D overexpression ($p < 0.001$), accompanied by a marked reduction in *PLCβ* expression ($p < 0.001$). Conversely, interference of *ADRA1D* led to a significant decrease in *ADRA1D* expression ($p < 0.001$) and a noteworthy increase in *PLCβ* expression ($p < 0.001$) (Fig. 6B). Moreover, WB analysis illustrated a significant increase in ADRA1D expression with overexpression of *ADRA1D* in PC12 cells ($p < 0.001$), coupled with a significant decrease in PLCβ and IP3R expression ($p < 0.05$). Conversely, interference of *ADRA1D* resulted in a significant decrease in ADRA1D expression ($p < 0.001$) and a significant increase in PLCβ and IP3R expression ($p < 0.05$) (Fig. 6C). Fluo-3AM was also employed to assess intracellular Ca^{2+} content in PC12 cells. The x-axis represents the mean fluo-

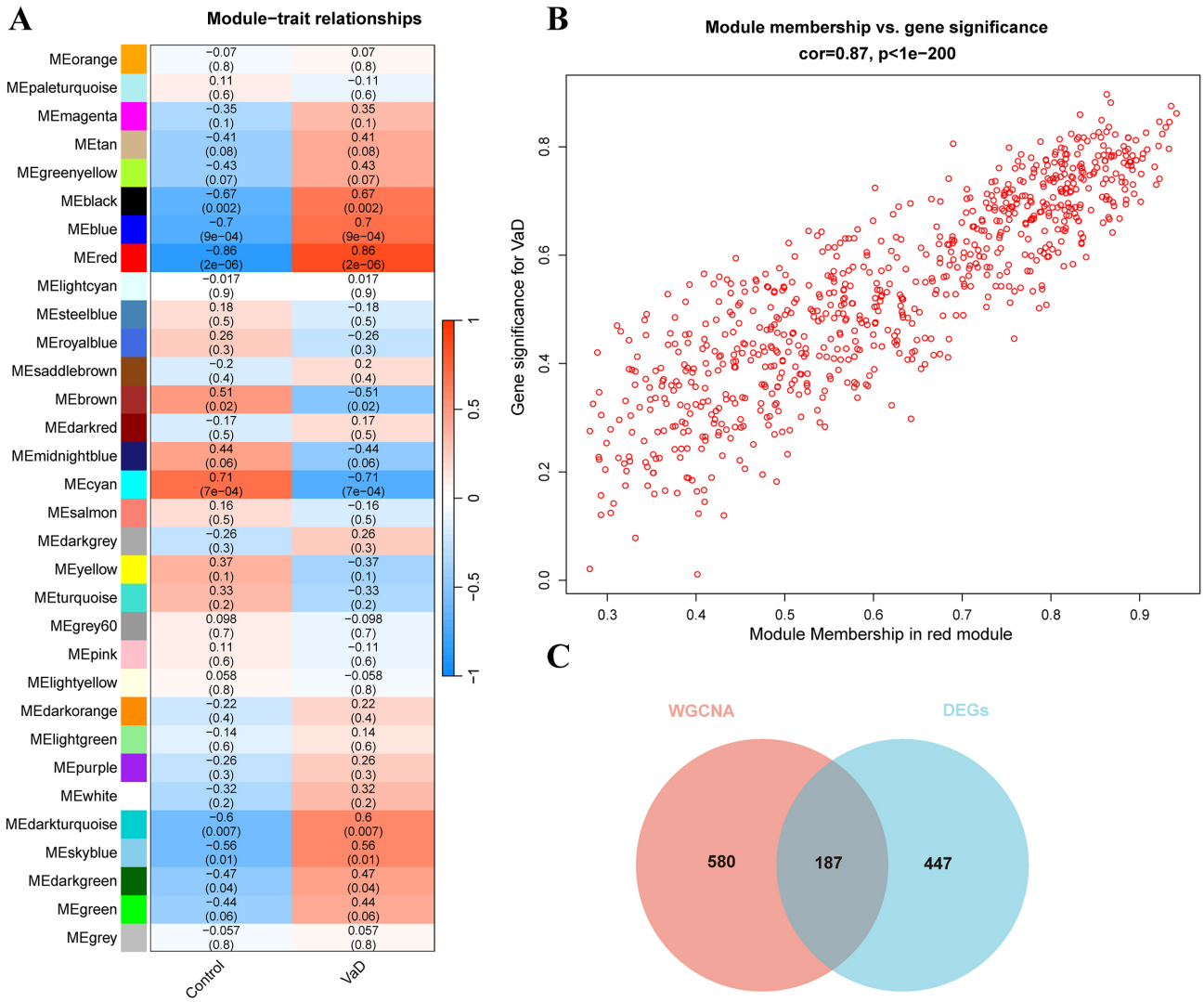

Fig. 3. Identification of modules associated with the clinical traits of VaD. (A) Heatmap of the correlation between module eigengenes and clinical traits of VaD. (B) There is a significant correlation between the key module (red module) and VaD. (C) Venn diagram of red module genes with DEGs.

rescence intensity, while the y-axis represents the number of cells. Overexpression of *ADRA1D* significantly diminished the Ca^{2+} content ($p < 0.001$), whereas interference of *ADRA1D* led to a substantial increase in Ca^{2+} content ($p < 0.001$) (Fig. 7).

Discussion

VaD, a clinical syndrome characterized by cognitive impairment resulting from cerebrovascular diseases, is the second most prevalent type of dementia after AD [22]. The pathogenesis of VaD is intricate and involves various factors, such as cerebrovascular diseases, aging, and diabetes, which collectively contribute to cerebral white matter dysfunction and significant regression of higher cortical functions [23]. Understanding the molecular mechanisms underlying VaD onset is crucial for developing effective prevention and treatment strategies. Consequently, large-scale gene expression profiling of VaD patients using gene chip technology, combined with bioinformatics analysis, can facilitate the identification of hub genes and the selection of viable therapeutic targets, thereby aiding in developing effective treatments for VaD [24]. In this study, we conducted bioinformatics analyses on gene expression patterns in frontal cortex samples from VaD patients, identifying 634 differentially expressed genes (DEGs) between VaD and normal samples. Further WGCNA analysis revealed 187 DEGs strongly correlated with VaD in the red module. GO and KEGG enrichment analyses highlighted pathways

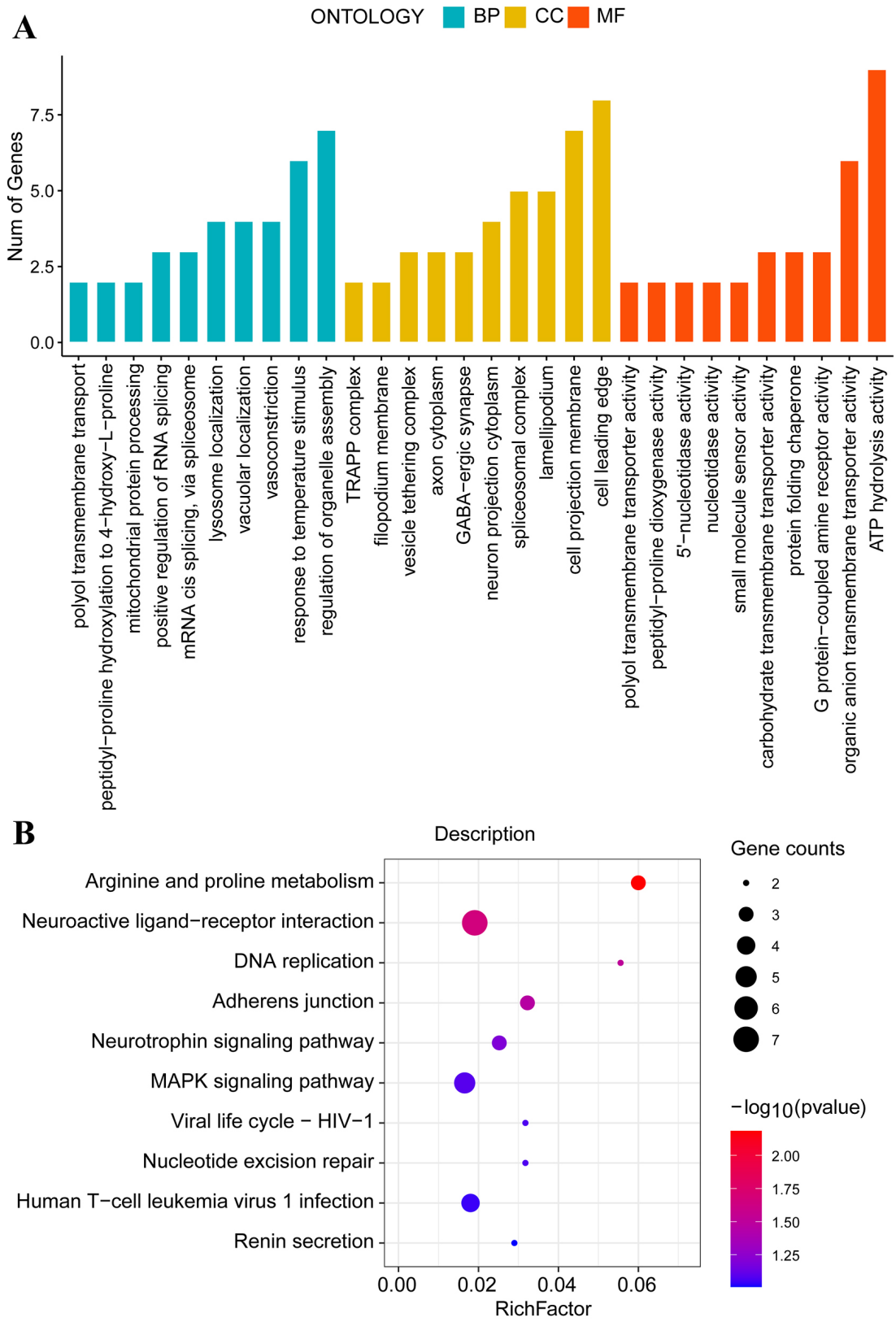

Fig. 4. Gene ontology and pathway enrichment analysis of red module genes. (A) The bar chart of the top 10 Gene Ontology (GO) enrichment terms. BP, biological processes; CC, cellular components; MF, molecular functions. (B) The dot chart of the top 10 Kyoto Encyclopedia of Genes and Genomes (KEGG) pathways.

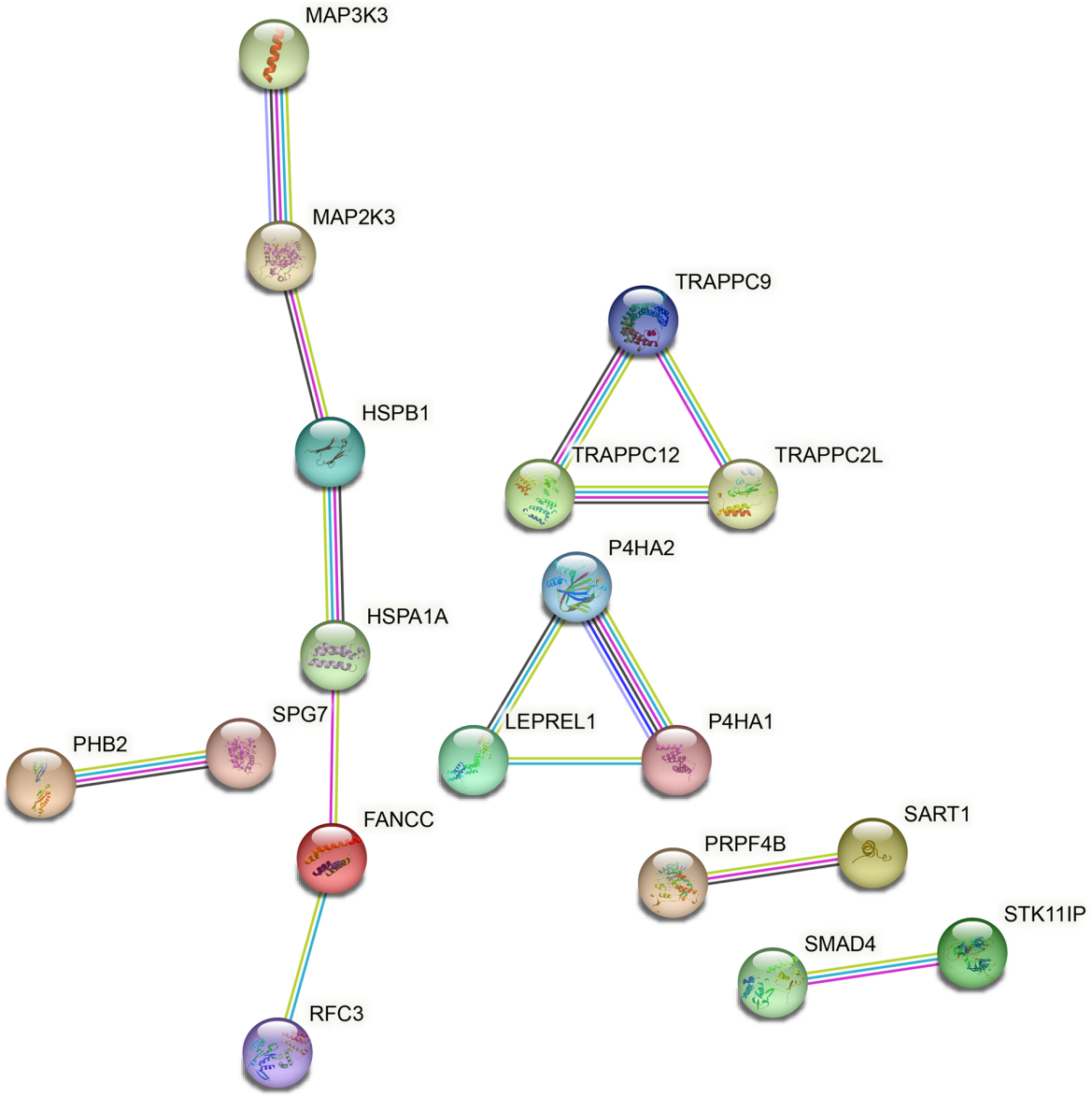

Fig. 5. Network plot of key genes in the red module; nodes indicate genes.

related to vasoconstriction, G protein-coupled amine receptor activity, neuroactive ligand-receptor interaction, MAPK signaling pathway, and adherens junctions.

Recent study has implicated prolonged glucose and oxygen deprivation in neurovascular unit damage, leading to VaD via vasoconstriction [25]. Chen *et al.* [26] identified DEGs associated with Danshen treatment for VaD, enriching in GO terms such as G protein-coupled amine receptor activity. Li *et al.*'s [27] research revealed that key targets of acupuncture therapy (AT) treatment for VaD were enriched in pathways like Neuroactive ligand-receptor interaction, mirroring our findings. Increasing evidence has suggested that the MAPK signaling pathway plays a critical role in the progression of VaD, with improvement in both AD and VaD linked to the inhibition or inactivation of the p38 MAPK pathway [28]. Additionally, emerging studies have indicated the potential involvement of adherent junctions in VaD development. Patients with AD and VaD often exhibit changes in brain microcirculation, including loss of tight and adherent junctions and increased blood-brain barrier permeability [29], which is believed to be a consequence of altered adherent junctions [30]. We conducted a PPI analysis to further understand the pathogenic mechanisms and identify potential therapeutic targets in VaD. Among the 187 DEGs identified in the robust red module of WGCNA, 18 hub genes were found to have protein-protein interactions, including *FANCC*, *HSPA1A*, *HSPB1*, *LEPREL1*,

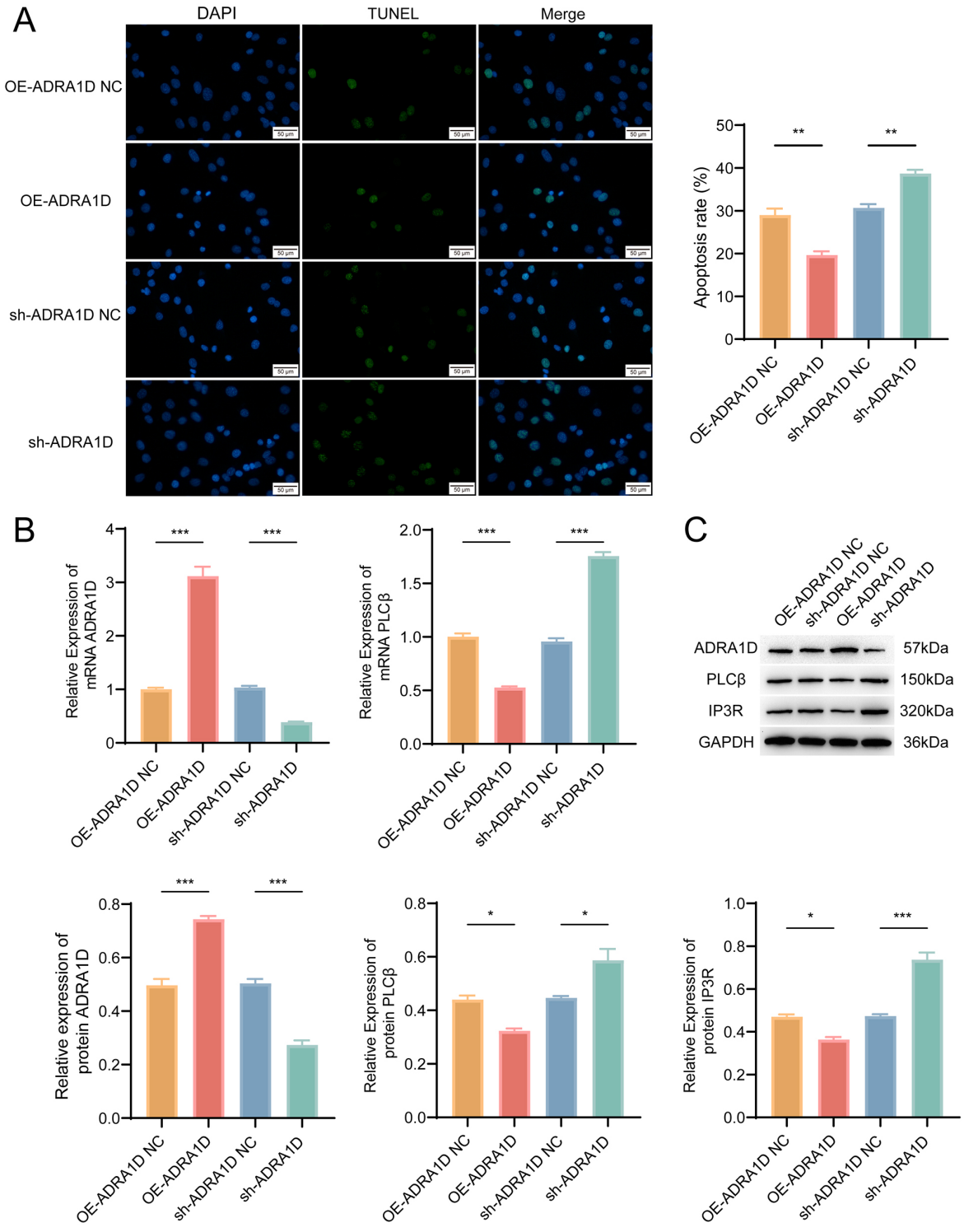

Fig. 6. Impact of overexpression and interference of adrenoceptor alpha 1D (*ADRA1D*) on apoptosis and Ca^{2+} homeostasis in oxygen-glucose deprivation (OGD) model pheochromocytoma 12 (PC12) cells. (A) TdT-mediated dUTP nick end labeling (TUNEL) assay depicting PC12 cell apoptosis. (B) Reverse transcription-quantitative polymerase chain reaction (RT-qPCR) examining the influence of overexpression and interference of *ADRA1D* on mRNA expression of *ADRA1D* and phospholipase C beta (*PLCβ*) in PC12 cells. (C) Western blot assessing the impact of overexpression and silencing of *ADRA1D* on protein expression of ADRA1D, inositol 1,4,5-trisphosphate receptor (IP3R), and PLCβ in PC12 cells. *$p < 0.05$, **$p < 0.01$, ***$p < 0.001$ compared to OE-*ADRA1D* NC or sh-*ADRA1D* NC. n = 3. GAPDH, Glyceraldehyde-3-phosphate dehydrogenase.

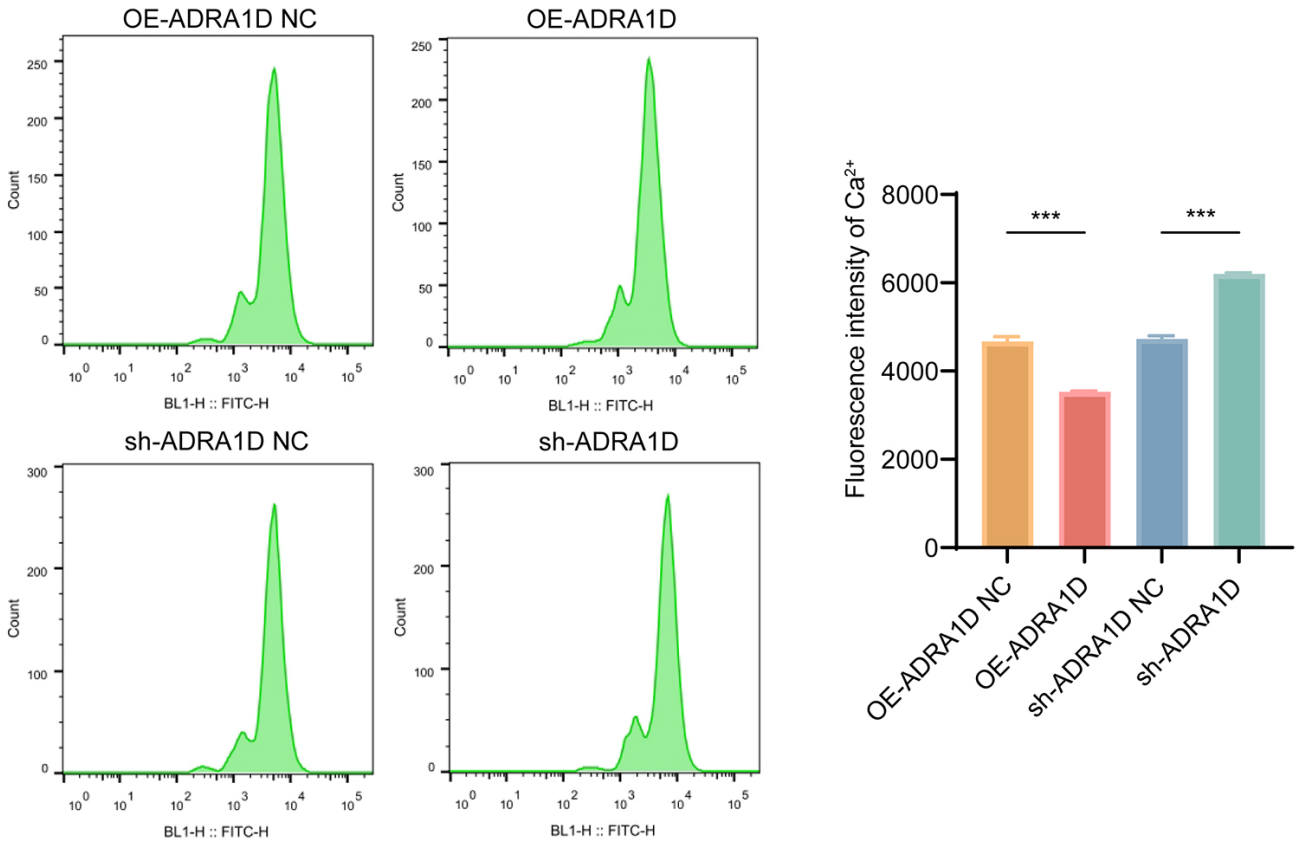

Fig. 7. Fluo-3-pentaacetoxymethyl ester (Fluo-3AM) measurement illustrates the effect of overexpression and silencing of *ADRA1D* on intracellular calcium ion levels in PC12 cells. ***$p < 0.001$ compared to OE-*ADRA1D* NC or sh-*ADRA1D* NC. n = 3.

MAP2K3, *MAP3K3*, *P4HA1*, *P4HA2*, *PHB2*, Pre-MRNA Processing Factor 4B (*PRPF4B*), *RFC3*, *SART1*, *SMAD4*, *SPG7*, *STK11IP*, *TRAPPC12*, *TRAPPC2L*, *TRAPPC9*.

The core pathogenic factor of VaD is believed to be cerebrovascular disease, leading to hypoxia, phosphorylation of tau protein, β-amyloid accumulation, blood-brain barrier dysfunction, and neuronal degeneration [31,32]. Factors like oxidative stress, cell apoptosis, and inflammatory responses are also implicated in VaD pathogenesis [33]. Studies have also shown that specific biomarkers correlated with inflammation and oxidative stress have emerged as potential indicators of VaD [13,18]. FANCC, a fanconi anemia (FA) protein family member, is involved in cellular stress responses, including DNA damage and oxidative stress [34]. Heat shock proteins (HSPs) are a group of proteins that accumulate in cells after heat shock and possess heat resistance characteristics that are generated in large quantities during cellular damage or conditions such as heat stress and oxidative stress [35]. Research suggests that *HSPA1A* regulates the JNK/p38 pathway within the MAPK signaling pathway and can inhibit apoptosis induced by this pathway [36]. *HSPB1*, a potential anti-inflammatory gene, represents a compensatory response to pro-inflammatory reactions [37]. PRPF4B, a kinase belonging to the Cell Division Cycle-like Kinase (CLK) protein kinase family [38]. Studies have demonstrated that silencing *PRPF4B* increases apoptosis in pancreatic cancer cell lines [39]. RFC3 is a small subunit of the RFC complex initially purified from HeLa cells and plays a critical role in DNA replication, DNA damage repair, and checkpoint control [40]. Downregulation of *RFC3* expression has been shown to induce cell cycle arrest in the S phase and trigger apoptosis in OVCAR-3 cells [41]. VaD development is related to cell apoptosis, which is in accordance with our findings. P4HA1 and P4HA2 are rate-limiting subunits of prolyl 4-hydroxylase (P4H) [42]. Study has indicated that the expression of P4HA1 and P4HA2 is associated with chronic hypoxia and is linked to AD [43]. Chronic hypoxia contributes to VaD, which is consistent with our results. MAP2K3 is a member of the MAPK family [44]. Increasing evidence has suggested that targeting MAP2K3 to block the MAPK signaling pathway can prevent blood-brain barrier damage and be beneficial for treating cerebral ischemia

[45]. MAP3K3 is a serine/threonine protein kinase belonging to the MAP3K subfamily [46], and study has shown its association with cerebrovascular diseases [47]. SMAD4 is a protein group that transmits extracellular signals directly to the cell nucleus [48]. Recent research has reported that endothelial-specific knockout of *SMAD4* leads to blood-brain barrier disruption and severe bleeding [49]. Blood-brain barrier damage and cerebrovascular diseases are important factors contributing to VaD, consistent with our results. Therefore, the identified hub genes are implicated in VaD development through their roles in cellular stress responses, DNA repair, hypoxia-related pathways, and blood-brain barrier integrity. Additionally, the involvement of proteins like PHB2, STK11IP, and SPG7 in mitochondrial processes suggests a link between mitochondrial dysfunction and neurodegenerative diseases like Parkinson's disease and AD, which may also impact VaD development [50–55]. However, further exploration is needed to investigate the potential of these identified targets as therapeutic ones for VaD treatment.

We identified *ADRA1D* as a DEG shared among vasoconstriction, G protein-coupled amine receptor activity, and the neuroactive ligand-receptor interaction. Previous studies have suggested that *ADRA1D* plays a role in controlling vascular constriction [56]. The alpha-D1 adrenergic receptor encoded by *ADRA1D* is downregulated in the hippocampus of Alzheimer's disease and Lewy body dementia patients [57]. Li *et al.* [27] identified *ADRA1D* as a key target in acupuncture treatment for VaD through WGCNA. Therefore, *ADRA1D* may play a crucial role in the physiological processes of VaD. However, the specific biological mechanisms remain unclear. The OGD model is commonly employed to simulate pathological changes at the cellular level, mimicking the pathophysiological alterations associated with VaD and other brain ischemia-hypoxia-induced damages [58]. It is well-known that abnormal intracellular calcium homeostasis is a primary pathological mechanism in brain ischemia-induced VaD [59], and the loss of calcium ion balance plays a significant role in ischemia-induced neuronal injury [60]. The phospholipase C (PLC)/inositol triphosphate (IP3) pathway can mediate neuronal apoptosis in brain tissue and play a neuroprotective role. PLCβ can be activated by G protein-coupled receptors, hydrolyzing phosphatidylinositol-4,5-bisphosphate (PIP2) into diacylglycerol (DAG) and inositol trisphosphate (IP3) [61]. DAG and IP3 are important second messengers that can activate protein kinase C, release calcium ions, and regulate cell apoptosis, as well as modulate the physiological effects of neuronal growth, differentiation, and survival [62]. By overexpressing and silencing *ADRA1D* in OGD-induced PC12 cells, we investigated its impact on cell apoptosis and Ca^{2+} balance. The results indicate that overexpression of *ADRA1D* significantly inhibits OGD-induced PC12 cell apoptosis and decreases intracellular Ca^{2+} levels by suppressing the PLC/IP3 pathway. This suggests a potential role for *ADRA1D* in alleviating cell damage induced by oxygen-glucose deprivation. Conversely, interference with *ADRA1D* yielded opposite results. However, the study still has some limitations, such as lacking *in vivo* verification of the gene *ADRA1D*, as findings from *in vitro* studies may not fully capture the complex interactions and effects of the gene in a living organism. The study acknowledges the need for further exploration to investigate the potential of the identified targets, including *ADRA1D*, as therapeutic candidates for VaD treatment. This highlights the preliminary nature of the findings and the necessity for additional research to confirm the therapeutic relevance of the identified genes.

Conclusion

In conclusion, DEGs associated with VaD are significantly enriched in pathways such as vasoconstriction, G protein-coupled amine receptor activity, neuroactive ligand-receptor interaction, and MAPK signaling pathway, which play crucial roles in the progression of VaD. The gene *ADRA1D*, shared among vasoconstriction, G protein-coupled amine receptor activity, and neuroactive ligand-receptor interaction, significantly inhibits apoptosis in OGD-induced PC12 cells. This effect is achieved by suppressing the PLC/IP3 pathway, reducing intracellular Ca^{2+} levels, and alleviating cellular damage induced by oxygen-glucose deprivation. Our study provides potential therapeutic targets for intervention in VaD. However, further *in vivo* validation is necessary for future developments.

Availability of Data and Materials

All data supporting the findings are included in the article. The datasets used and/or analyzed during the current study are available from the corresponding authors on reasonable request.

Author Contributions

QSH, ABZ, YHW, and JC designed the research study. YHW and JC performed the research. BP and LPC provided help and advice on the TUNEL experiments. QKH were involved in the acquisition of data. QSH and ABZ interpreted the data and critically reviewed the manuscript. All authors contributed to editorial changes

in the manuscript. All authors read and approved the final manuscript. All authors have participated sufficiently in the work and agreed to be accountable for all aspects of the work.

Ethics Approval and Consent to Participate

Not applicable.

Acknowledgment

Not applicable.

Funding

This research was supported by the Regional Science Foundation Project of National Natural Science Foundation of China: Exploration of the mechanism of acupuncture on Du Channel to improve cognitive function in vascular dementia based on the regulation of mitochondrial autophagy by the PINK1/Parkin pathway (NO. 82260970).

Conflict of Interest

The authors declare no conflict of interest.

Supplementary Material

Supplementary material associated with this article can be found, in the online version, at https://doi.org/10.62641/aep.v52i2.1601.

References

[1] Weidner W, Barbarino P. The State of the Art of Dementia Research: New Frontiers. Alzheimer's & Dementia. 2019; 15: P1473.

[2] Lai NM, Chang SMW, Ng SS, Tan SL, Chaiyakunapruk N, Stanaway F. Animal-assisted therapy for dementia. The Cochrane Database of Systematic Reviews. 2019; 2019: CD013243.

[3] Wolters FJ, Ikram MA. Epidemiology of Vascular Dementia. Arteriosclerosis, Thrombosis, and Vascular Biology. 2019; 39: 1542–1549.

[4] Jia L, Quan M, Fu Y, Zhao T, Li Y, Wei C, *et al*. Dementia in China: epidemiology, clinical management, and research advances. The Lancet. Neurology. 2020; 19: 81–92.

[5] Li L, Zheng Y, Bao J, Zhao Y, Zhang Q, Li W, *et al*. Meta-Analysis of Naoxintong Capsule for Patients with Vascular Dementia. Evidence-based Complementary and Alternative Medicine: eCAM. 2022; 2022: 5000948.

[6] Román GC. Vascular dementia. Advances in nosology, diagnosis, treatment and prevention. Panminerva Medica. 2004; 46: 207–215.

[7] Fang M, Li J, Tiu SC, Zhang L, Wang M, Yew DT. N-methyl-D-aspartate receptor and apoptosis in Alzheimer's disease and multiinfarct dementia. Journal of Neuroscience Research. 2005; 81: 269–274.

[8] Wen J, Cao Y, Chang S, Huang Q, Zhang Z, Wei W, *et al*. A network meta-analysis on the improvement of cognition in patients with vascular dementia by different acupuncture therapies. Frontiers in Neuroscience. 2022; 16: 1053283.

[9] Tukacs V, Mittli D, Györffy BA, Hunyady-Gulyás É, Hlatky D, Tóth V, *et al*. Chronic stepwise cerebral hypoperfusion differentially induces synaptic proteome changes in the frontal cortex, occipital cortex, and hippocampus in rats. Scientific Reports. 2020; 10: 15999.

[10] Kalaria RN. The pathology and pathophysiology of vascular dementia. Neuropharmacology. 2018; 134: 226–239.

[11] Li D, Huang Z, Dai Y, Guo L, Lin S, Liu X. Bioinformatic identification of potential biomarkers and therapeutic targets in carotid atherosclerosis and vascular dementia. Frontiers in Neurology. 2023; 13: 1091453.

[12] Luo J, Chen L, Huang X, Xie J, Zou C, Pan M, *et al*. REPS1 as a Potential Biomarker in Alzheimer's Disease and Vascular Dementia. Frontiers in Aging Neuroscience. 2022; 14: 894824.

[13] Hosoki S, Tanaka T, Ihara M. Diagnostic and prognostic blood biomarkers in vascular dementia: From the viewpoint of ischemic stroke. Neurochemistry International. 2021; 146: 105015.

[14] Malhotra S, Costa C, Eixarch H, Keller CW, Amman L, Martínez-Banaclocha H, *et al*. NLRP3 inflammasome as prognostic factor and therapeutic target in primary progressive multiple sclerosis patients. Brain: a Journal of Neurology. 2020; 143: 1414–1430.

[15] Custodero C, Ciavarella A, Panza F, Gnocchi D, Lenato GM, Lee J, *et al*. Role of inflammatory markers in the diagnosis of vascular contributions to cognitive impairment and dementia: a systematic review and meta-analysis. GeroScience. 2022; 44: 1373–1392.

[16] Sergi D, Zauli E, Tisato V, Secchiero P, Zauli G, Cervellati C. Lipids at the Nexus between Cerebrovascular Disease and Vascular Dementia: The Impact of HDL-Cholesterol and Ceramides. International Journal of Molecular Sciences. 2023; 24: 4403.

[17] Kartavenka K, Panuwet P, Yakimavets V, Jaikang C, Thipubon K, D'Souza PE, *et al*. LC-MS Quantification of Malondialdehyde-Dansylhydrazine Derivatives in Urine and Serum Samples. Journal of Analytical Toxicology. 2020; 44: 470–481.

[18] Taler-Verčič A, Goličnik M, Bavec A. The Structure and Function of Paraoxonase-1 and Its Comparison to Paraoxonase-2 and -3. Molecules (Basel, Switzerland). 2020; 25: 5980.

[19] Gao XZ, Ma RH, Zhang ZX. miR-339 Promotes Hypoxia-Induced Neuronal Apoptosis and Impairs Cell Viability by Targeting FGF9/CACNG2 and Mediating MAPK Pathway in Ischemic Stroke. Frontiers in Neurology. 2020; 11: 436.

[20] Wang M, Dai M, Wu YS, Yi Z, Li Y, Ren G. Immunoglobulin superfamily member 10 is a novel prognostic biomarker for breast cancer. PeerJ. 2020; 8: e10128.

[21] Szklarczyk D, Gable AL, Lyon D, Junge A, Wyder S, Huerta-Cepas J, *et al*. STRING v11: protein-protein association networks with increased coverage, supporting functional discovery in genome-wide

experimental datasets. Nucleic Acids Research. 2019; 47: D607–D613.

[22] Karamacoska D, Chan DKY, Leung I, Liu JX, Brodaty H, Fahey PP, *et al*. Study protocol for a phase III randomised controlled trial of Sailuotong (SLT) for vascular dementia and Alzheimer's disease with cerebrovascular disease. PloS One. 2023; 18: e0265285.

[23] Román G. Vascular dementia: a historical background. International Psychogeriatrics. 2003; 15: 11–13.

[24] Shu J, Wei W, Zhang L. Identification of Molecular Signatures and Candidate Drugs in Vascular Dementia by Bioinformatics Analyses. Frontiers in Molecular Neuroscience. 2022; 15: 751044.

[25] Sabogal-Guáqueta AM, Villamil-Ortiz JG, Arias-Londoño JD, Cardona-Gómez GP. Inverse Phosphatidylcholine/Phosphatidylinositol Levels as Peripheral Biomarkers and Phosphatidylcholine/Lysophosphatidylethanolamine-Phosphatidylserine as Hippocampal Indicator of Postischemic Cognitive Impairment in Rats. Frontiers in Neuroscience. 2018; 12: 989.

[26] Chen J, Chen W, Tang XS, Wu Y, Lao WL, Wu L. To explore the mechanism of Danshen in the treatment of vascular dementia based on network pharmacology. Western Chinese Medicine. 2022; 35: 22–31. (In Chinese)

[27] Li D, Yang H, Lyu M, Wang J, Xu W, Wang Y. Acupuncture Therapy on Dementia: Explained with an Integrated Analysis on Therapeutic Targets and Associated Mechanisms. Journal of Alzheimer's Disease: JAD. 2023; 94: S141–S158.

[28] Wei TH, Hsieh CL. Effect of Acupuncture on the p38 Signaling Pathway in Several Nervous System Diseases: A Systematic Review. International Journal of Molecular Sciences. 2020; 21: 4693.

[29] Sandsmark DK, Bashir A, Wellington CL, Diaz-Arrastia R. Cerebral Microvascular Injury: A Potentially Treatable Endophenotype of Traumatic Brain Injury-Induced Neurodegeneration. Neuron. 2019; 103: 367–379.

[30] Binda A, Murano C, Rivolta I. Innovative Therapies and Nanomedicine Applications for the Treatment of Alzheimer's Disease: A State-of-the-Art (2017-2020). International Journal of Nanomedicine. 2020; 15: 6113–6135.

[31] Liuzzo JP, Petanceska SS, Moscatelli D, Devi LA. Inflammatory mediators regulate cathepsin S in macrophages and microglia: A role in attenuating heparan sulfate interactions. Molecular Medicine (Cambridge, Mass.). 1999; 5: 320–333.

[32] Pluta R, Miziak B, Czuczwar SJ. Post-Ischemic Permeability of the Blood-Brain Barrier to Amyloid and Platelets as a Factor in the Maturation of Alzheimer's Disease-Type Brain Neurodegeneration. International Journal of Molecular Sciences. 2023; 24: 10739.

[33] Dallali H, Boukhalfa W, Kheriji N, Fassatoui M, Jmel H, Hechmi M, *et al*. The first exome wide association study in Tunisia: identification of candidate loci and pathways with biological relevance for type 2 diabetes. Frontiers in Endocrinology. 2023; 14: 1293124.

[34] Kaljunen H, Taavitsainen S, Kaarijärvi R, Takala E, Paakinaho V, Nykter M, *et al*. Fanconi anemia pathway regulation by FANCI in prostate cancer. Frontiers in Oncology. 2023; 13: 1260826.

[35] Joly AL, Wettstein G, Mignot G, Ghiringhelli F, Garrido C. Dual role of heat shock proteins as regulators of apoptosis and innate immunity. Journal of Innate Immunity. 2010; 2: 238–247.

[36] Gholizadeh MA, Shamsabadi FT, Yamchi A, Golalipour M, Jhingan GD, Shahbazi M. Identification of hub genes associated with RNAi-induced silencing of XIAP through targeted proteomics approach in MCF7 cells. Cell & Bioscience. 2020; 10: 78.

[37] Ogbodo E, Michelangeli F, Williams JHH. Exogenous heat shock proteins HSPA1A and HSPB1 regulate TNF-α, IL-1β and IL-10 secretion from monocytic cells. FEBS Open Bio. 2023; 13: 1922–1940.

[38] Islam SU, Shehzad A, Sonn JK, Lee YS. PRPF overexpression induces drug resistance through actin cytoskeleton rearrangement and epithelial-mesenchymal transition. Oncotarget. 2017; 8: 56659–56671.

[39] Blijlevens M, Li J, van Beusechem VW. Biology of the mRNA Splicing Machinery and Its Dysregulation in Cancer Providing Therapeutic Opportunities. International Journal of Molecular Sciences. 2021; 22: 5110.

[40] Piran M, Sepahi N, Moattari A, Rahimi A, Ghanbariasad A. Systems Biomedicine of Primary and Metastatic Colorectal Cancer Reveals Potential Therapeutic Targets. Frontiers in Oncology. 2021; 11: 597536.

[41] Shen H, Xu J, Zhao S, Shi H, Yao S, Jiang N. ShRNA-mediated silencing of the RFC3 gene suppress ovarian tumor cells proliferation. International Journal of Clinical and Experimental Pathology. 2015; 8: 8968–8975.

[42] Xu Y, Xia D, Huang K, Liang M. Hypoxia-induced P4HA1 overexpression promotes post-ischemic angiogenesis by enhancing endothelial glycolysis through downregulating FBP1. Journal of Translational Medicine. 2024; 22: 74.

[43] Fiorenzano A, Sozzi E, Birtele M, Kajtez J, Giacomoni J, Nilsson F, *et al*. Single-cell transcriptomics captures features of human midbrain development and dopamine neuron diversity in brain organoids. Nature Communications. 2021; 12: 7302.

[44] Zhou F, Xu Y, Hou XY. MLK3-MKK3/6-P38MAPK cascades following N-methyl-D-aspartate receptor activation contributes to amyloid-β peptide-induced apoptosis in SH-SY5Y cells. Journal of Neuroscience Research. 2014; 92: 808–817.

[45] He F, Xiao Z, Yao H, Li S, Feng M, Wang W, *et al*. The protective role of microRNA-21 against coxsackievirus B3 infection through targeting the MAP2K3/P38 MAPK signaling pathway. Journal of Translational Medicine. 2019; 17: 335.

[46] Hu Q, Shen W, Huang H, Liu J, Zhang J, Huang X, *et al*. Insight into the binding properties of MEKK3 PB1 to MEK5 PB1 from its solution structure. Biochemistry. 2007; 46: 13478–13489.

[47] Li M, Ke J, Deng Y, Chen C, Huang Y, Bian Y, *et al*. The Protective Effect of Liquiritin in Hypoxia/Reoxygenation-Induced Disruption on Blood Brain Barrier. Frontiers in Pharmacology. 2021; 12: 671783.

[48] Budi EH, Duan D, Derynck R. Transforming Growth Factor-β Receptors and Smads: Regulatory Complexity and Functional Versatility. Trends in Cell Biology. 2017; 27: 658–672.

[49] Thalgott J, Dos-Santos-Luis D, Lebrin F. Pericytes as targets in hereditary hemorrhagic telangiectasia. Frontiers in Genetics. 2015; 6: 37.

[50] Zeczycki TN, Maurice MS, Attwood PV. Inhibitors of Pyruvate Carboxylase. The Open Enzyme Inhibition Journal. 2010; 3: 8–26.

[51] Cirilo PDR, de Sousa Andrade LN, Corrêa BRS, Qiao M, Furuya

TK, Chammas R, *et al*. MicroRNA-195 acts as an anti-proliferative miRNA in human melanoma cells by targeting Prohibitin 1. BMC Cancer. 2017; 17: 750.

[52] Zi Z, Zhang Z, Feng Q, Kim C, Wang XD, Scherer PE, *et al*. Quantitative phosphoproteomic analyses identify STK11IP as a lysosome-specific substrate of mTORC1 that regulates lysosomal acidification. Nature Communications. 2022; 13: 1760.

[53] Yi L, Liu B, Nixon PJ, Yu J, Chen F. Recent Advances in Understanding the Structural and Functional Evolution of FtsH Proteases. Frontiers in Plant Science. 2022; 13: 837528.

[54] Mamelak M. Energy and the Alzheimer brain. Neuroscience and Biobehavioral Reviews. 2017; 75: 297–313.

[55] Ashraf GM, Chibber S, Mohammad, Zaidi SK, Tabrez S, Ahmad A, *et al*. Recent Updates on the Association Between Alzheimer's Disease and Vascular Dementia. Medicinal Chemistry (Shariqah (United Arab Emirates)). 2016; 12: 226–237.

[56] Takeuchi F, Liang YQ, Isono M, Tajima M, Cui ZH, Iizuka Y, *et al*. Integrative genomic analysis of blood pressure and related phenotypes in rats. Disease Models & Mechanisms. 2021; 14: dmm048090.

[57] Xicoy H, Brouwers JF, Wieringa B, Martens GJM. Explorative Combined Lipid and Transcriptomic Profiling of Substantia Nigra and Putamen in Parkinson's Disease. Cells. 2020; 9: 1966.

[58] Zhao T, Fu Y, Sun H, Liu X. Ligustrazine suppresses neuron apoptosis via the Bax/Bcl-2 and caspase-3 pathway in PC12 cells and in rats with vascular dementia. IUBMB Life. 2018; 70: 60–70.

[59] Nimmrich V, Eckert A. Calcium channel blockers and dementia. British Journal of Pharmacology. 2013; 169: 1203–1210.

[60] Bano D, Nicotera P. Ca2+ signals and neuronal death in brain ischemia. Stroke. 2007; 38: 674–676.

[61] Bernard A, Danigo A, Bourthoumieu S, Mroué M, Desmoulière A, Sturtz F, *et al*. The Cholecystokinin Type 2 Receptor, a Pharmacological Target for Pain Management. Pharmaceuticals (Basel, Switzerland). 2021; 14: 1185.

[62] Melo CV, Okumoto S, Gomes JR, Baptista MS, Bahr BA, Frommer WB, *et al*. Spatiotemporal resolution of BDNF neuroprotection against glutamate excitotoxicity in cultured hippocampal neurons. Neuroscience. 2013; 237: 66–86.